

**One-pot precipitation polymerisation strategy for tuneable injectable Laponite®-pNIPAM hydrogels: Polymerisation, processability and beyond**

BOYES, V.L., JANANI, Ronak <<http://orcid.org/0000-0002-3633-0488>>, PARTRIDGE, S., FIELDING, L.A. <<http://orcid.org/0000-0002-4958-1155>>, BREEN, C., FOULKES, J., LE MAITRE, Christine <<http://orcid.org/0000-0003-4489-7107>> and SAMMON, Chris <<http://orcid.org/0000-0003-1714-1726>>

Available from Sheffield Hallam University Research Archive (SHURA) at:  
<https://shura.shu.ac.uk/29202/>

---

This document is the Accepted Version [AM]

**Citation:**

BOYES, V.L., JANANI, Ronak, PARTRIDGE, S., FIELDING, L.A., BREEN, C., FOULKES, J., LE MAITRE, Christine and SAMMON, Chris (2021). One-pot precipitation polymerisation strategy for tuneable injectable Laponite®-pNIPAM hydrogels: Polymerisation, processability and beyond. *Polymer*, 233, p. 124201. [Article]

---

**Copyright and re-use policy**

See <http://shura.shu.ac.uk/information.html>

# One-Pot Precipitation Polymerisation Strategy for Tuneable Injectable Laponite<sup>®</sup>-pNIPAM Hydrogels: Polymerisation, Processability and Beyond.

Victoria L Boyes<sup>1</sup>, Ronak Janani<sup>2</sup>, Simon Partridge<sup>3</sup>, Lee A Fielding<sup>4</sup>, Christopher Breen<sup>2</sup>, Jonathan Foulkes<sup>5</sup>, Christine L Le Maitre<sup>6</sup>, Chris Sammon<sup>2\*</sup>

\* Corresponding author. Email: c.sammon@shu.ac.uk

<sup>1</sup> Biomaterials, Biomimetics and Biophotonics division, Floor 17 Tower Wing, Guy's Hospital, Great Maze Pond, SE1 9RT

<sup>2</sup> Materials and Engineering Research Institute, Sheffield Hallam University, Howard St, Sheffield, S1 1WB, UK

<sup>3</sup> Ivy Farm Technologies, Oxford, Oxfordshire, OX5 1PF

<sup>4</sup> Department of Materials & Henry Royce Institute, The University of Manchester, Manchester, M13 9PL, UK

<sup>5</sup> Tullis Russell Group, Church St, Bollington, Macclesfield, SK10 5QF, UK

<sup>6</sup> Biomolecular Sciences Research Centre, Sheffield Hallam University, Howard St, Sheffield, S1 1WB, UK

## Abstract

Highly processable hydrogels loaded with active components for localised drug delivery and/or live cells for regenerative medicine are an attractive target for biotechnology research. We describe a single-pot precipitation polymerisation of poly (N-isopropylacrylamide) (pNIPAM) from the surface of dispersed Laponite<sup>®</sup> platelets in aqueous media above its lower critical solution temperature (LCST), yielding tightly packed pNIPAM globules that resist aggregation and can be maintained for long periods of time as a low viscosity colloidal suspension. Upon cooling, the pNIPAM chains transform from the 'globule' to the 'coil' conformation, establishing multiple physical interactions and chain entanglement leading to irreversible gel formation. We have shown that the temperature and rate of phase transition and the rheological and mechanical properties of Laponite<sup>®</sup>-pNIPAM hydrogel can be tailored by addition of *N,N*-dimethylacrylamide (DMAc) comonomer and other biologically relevant additives. The tuneable properties of Laponite<sup>®</sup>-pNIPAM hydrogel confirms its excellent potential for a wide range of therapeutic applications.

Key Words: injectable hydrogel, regenerative medicine, localised drug delivery, lower critical solution temperature, thermoresponsive polymers.

## 1. Introduction

Development of hydrogel biomimetic materials with sol-gel (solution to solidification) properties that allow injection followed by spontaneous solidification has resulted in several classes of injectable hydrogel materials suitable for tissue engineering<sup>1-5</sup>. Researchers have examined self-assembly<sup>6-8</sup> Michael-type addition<sup>9-11</sup>, click chemistry (Diels-Alder cycloaddition, azide-nitrile addition, thiol-ene addition<sup>12-14</sup>) and disulphide<sup>15,16</sup>, photo-mediated<sup>17</sup>, ionic<sup>18,19</sup>, Schiff base<sup>20,21</sup>, and enzyme-mediated<sup>22-24</sup> crosslinking to achieve this. Some technologies exclude the use of potentially cytotoxic crosslinking agents and curing methods, allowing the mixing and simultaneous transplantation of live cells with a polymeric scaffold to the affected site<sup>25-27</sup>. This mode of delivery is a minimally invasive alternative to

implantation of pre-formed gels, which requires surgical placement and carries increased risk of infection and relatively poor margin adaptation. Injectable scaffolds are a favourable alternative as they offer reduced complication risk, scarring and pain, and can easily be delivered to deep tissues, with improved tissue/scaffold interfaces<sup>28</sup>.

Water-soluble, thermosensitive polymers such as poly(*N*-isopropylacrylamide) (pNIPAM) enable non-invasive implantation. Having a lower critical solution temperature (LCST) close to human physiological temperature has resulted in strong interest in pNIPAM for tissue engineering applications. Precipitation polymerisation techniques are typically employed for the synthesis of pNIPAM hydrogels, whereby the polymer is synthesised at high temperatures in the presence of a crosslinking agent containing two vinyl groups, e.g., *N,N*-methylenebisacrylamide (BIS), using a thermally-dissociating free-radical initiator. Since chain propagation results in the formation of hydrophobic regimes, the chains collapse to form tightly packed nanoaggregates. The covalent crosslinks that BIS provides ensure that the polymer chains do not unravel and dissolve when they become water soluble at temperatures lower than the LCST, but instead form discrete swollen microparticles. It has been suggested that, at sufficiently high solid content, pNIPAM forms self-crosslinks, to produce tertiary carbon atoms which form microgel particles without any additional crosslinking agent<sup>11,29</sup>.

The phase transition of thermosensitive polymers around their LCST has been associated with the balance between the hydrophilic (water-polymer) and hydrophobic (polymer-polymer) interactions available in the system. Tunability of LCST transition of a hydrogel system expands its application in the field of drug delivery. It is well understood that incorporation of hydrophilic or hydrophobic monomers into the polymer backbone enables one to modulate the LCST of the hydrogel<sup>30-32</sup>. However, information about the range of an LCST transition is often omitted which underestimates the complexity of the phase transition process. Understanding the phase transition rate is vital for injectable hydrogels and those used for drug delivery. For example, a slow LCST is required for a steady drug release<sup>31</sup>.

Clay polymer nanocomposite hydrogels are also of particular interest in biomedicine because of their tailorable, tissue-like mechanical properties as well as their ability to dynamically alter their internal structure<sup>33,34</sup>. Currently, they find numerous applications in drug delivery<sup>35-37</sup>, cell cultivation<sup>38,39</sup> and tissue engineering<sup>40</sup> research.

We have previously reported the development of an injectable hydrogel which utilises the thermo-responsive behaviour of pNIPAM together with its ability to electrostatically interact with synthetic Laponite<sup>®</sup> clay platelets<sup>41-43</sup>. The synthetic approach was extended to include the incorporation of a hydrophilic monomer (*N,N*-dimethylacrylamide (DMAc)) to increase the cloud point and associated solidification temperature of the material to one appropriate for injection and solidification within body cavities. The stable colloidal suspension was shown to be injectable above LCST through a 26G needle. Through cell viability studies, we have demonstrated that cells could survive, migrate through the hydrogel and deposit matrix<sup>44</sup>.

This work aims to provide a better understanding of the physical chemistry of these Laponite<sup>®</sup>-pNIPAM (L<sub>x</sub>-pNIPAM<sub>y</sub>) hydrogels. Real-time dynamic light scattering analysis was exploited to monitor the polymerisation process. Furthermore, the correlation between DMAc content and the LCST range, hydrogel mechanical properties, viscosity, and morphology was investigated. The LCST range was determined using a combination of turbidimetry, calorimetry and rheology to enable accurate evaluation of the phase transition temperature range. The processability of the hydrogel was also examined by incorporating different additives which include hyaluronic acid (HA), gelatin and Poly(lactic-co-glycolic (PLGA) into the body of the hydrogel prior to solidification. Deeper understanding of physiochemical properties of this hydrogel system enables translation of promising application-specific formulations.

## 2. Experimental

### 2.1 Materials

*N*-isopropylacrylamide, 99% (NIPAM) was kindly provided by KJ Chemicals Corporation and was used without any modification. *N, N*-dimethylacrylamide was purchased from Sigma-Aldrich and used without further treatment or purification. A synthetic hectorite clay, Laponite<sup>®</sup> (a registered trademark of BYK Additives) was used as received. Gelatin and lyophilised bovine vitreous humour HA were purchased from Fluka<sup>®</sup> Analytical and used without modification. 2,2'-azobisisobutyronitrile (AIBN) (Sigma-Aldrich) was recrystallised from methanol. Poly(lactic-co-glycolic) acid (PLGA, RG752H - 75:25 lactide: glycolide, I.V. 0.16–0.24) was supplied by Critical Pharmaceuticals and used as received. All water was deionised 18 MΩ.

### 2.2 Synthesis of the liquid polymer/Laponite<sup>®</sup> nanocomposite hydrogels

#### 2.2.1 Preparation of L<sub>x</sub>-pNIPAM<sub>y</sub> gels.

An exfoliated suspension of Laponite<sup>®</sup> in water was prepared by vigorous stirring of Laponite<sup>®</sup> in water for 24h at room temperature. The AIBN and NIPAM were added to the suspension and stirred for 1h. After passing the suspension through 5-8μm pore filter paper, polymerisation was performed at 80°C for 24h in a sealed glass vial with minimum headspace to reduce the potential for oxygen termination of the free radical reaction. The liquid suspension transforms to an opaque suspension typically after ≈25 minutes and at this point, it is capable of forming solid gels upon cooling. For subsequent experiments which required solid hydrogels, the warm, polymerised liquid gel was cooled to room temperature to induce solidification within a suitably shaped vessel prior to use. Exact hydrogel compositions utilised in this work are listed in Table 1.

---

Table 1. Composition (%)					
w/w) of the samples used in					
this paper including all the					
L <sub>x</sub> -pNIPAM <sub>y</sub> hydrogels. The					
subscripts indicate the wt%					
	Laponite <sup>®</sup>	NIPAM	DMAc	Additive <sup>^</sup>	H <sub>2</sub> O

---

of each component except for compositions containing DMAc where the subscripts indicate the %DMAc of the overall polymer content for simplicity. The superscripts <sup>\*CTR</sup> and <sup>+CTR</sup> are used to indicate control hydrogel formulations for the DMA analysis (section 3.8). Sample ID

L <sub>1.0</sub> -pNIPAM <sub>9.0</sub>	1.00	9.00	-	-	90.00
L-pNIPAM-co-DMAc <sub>5</sub>	1.00	8.55	0.45	-	90.00
L-pNIPAM-co-DMAc <sub>10</sub>	1.00	8.10	0.90	-	90.00
L-pNIPAM-co-DMAc <sub>13</sub>	1.00	7.83	1.17	-	90.00
L-pNIPAM-co-DMAc <sub>15</sub>	1.00	7.65	1.35	-	90.00
L-pNIPAM-co-DMAc <sub>20</sub>	1.00	7.20	1.80	-	90.00
L <sub>0.5</sub> -pNIPAM <sub>4.5</sub>	0.50	4.50	-	-	95.00
pNIPAM <sub>5.0</sub>	0.00	5.00	-	-	95.00
L <sub>0.5</sub>	0.50	0.00	-	-	99.50
L <sub>0.9</sub> -pNIPAM <sub>8.1</sub> G <sub>5.0</sub>	0.90	8.10	-	5.00	86.00
L <sub>0.8</sub> -pNIPAM <sub>7.2</sub> G <sub>10.0</sub>	0.80	7.20	-	10.00	82.00
L <sub>0.88</sub> -pNIPAM <sub>8.0</sub> <sup>+CTR</sup>	0.88	8.00	-	-	91.12
Gelatin <sub>10</sub>	-	-	-	10.00	90.00
L <sub>0.9</sub> -pNIPAM <sub>8.1</sub> HA <sub>0.2</sub>	0.90	8.10	-	0.20	90.80
L <sub>0.8</sub> -pNIPAM <sub>7.2</sub> HA <sub>0.4</sub>	0.80	7.20	-	0.40	91.60
L <sub>0.81</sub> -pNIPAM <sub>7.23</sub> <sup>*CTR</sup>	0.81	7.23	-	-	91.96
L <sub>0.9</sub> -pNIPAM <sub>8.1</sub> PLGA <sub>10</sub>	0.90	8.10	-	10.00	81.00

<sup>^</sup> Additive refers to mass of gelatin, hyaluronic acid, or PLGA.

### 2.2.2 Preparation of L-pNIPAM-co-DMAc<sub>x</sub> gels.

Synthesis followed the protocol described in 2.2.1 with the addition of dimethylacrylamide (DMAc) in the appropriate quantity to the monomeric suspension (see Table 1).

### 2.2.3 Preparation of L<sub>x</sub>-pNIPAM<sub>y</sub> gels containing gelatin additive.

The liquid hydrogel was synthesised as per 2.2.1/2.2.2. A gelatin solution was made by heating a 1:1 w/v mixture of gelatin and 18 MΩ deionised water to 70°C and stirred until dissolved. Measured quantities of this solution (as shown in Table 1) were combined with the liquid hydrogel and stirred in a heated ultrasonic bath (40 KHz at 70°C) for 30 minutes until the gelatin-containing hydrogel precursor formed a homogenous pale-yellow liquid.

#### 2.2.4 Preparation of L<sub>x</sub>-pNIPAM<sub>y</sub> gels containing HA additive.

The liquid hydrogel was synthesised as per 2.2.1/2.2.2. An aqueous HA solution was prepared by refrigerating a 50:1 w/v mixture of HA and 18 MΩ deionised water for 48 hours, during which time it was removed and stirred vigorously every 8 hours. Appropriate quantities of this solution required to provide the desired final formulations were then combined with the liquid hydrogel and stirred in a heated ultrasonic bath (40 KHz at 40°C) for 30 minutes until the HA-containing hydrogel precursor formed a homogenous milky liquid.

#### 2.2.5 Preparation of L<sub>x</sub>-pNIPAM<sub>y</sub> gel containing PLGA.

The L<sub>x</sub>-pNIPAM<sub>y</sub> containing 10% PLGA was prepared by vigorously stirring PLGA microparticles<sup>45</sup> into L<sub>1.0</sub>-pNIPAM<sub>9.0</sub> synthesised as per 2.2.1. The composition and identifying codes for each hydrogel composition are provided in Table 1.

### 2.3 Material Characterisation

#### 2.3.1 Dynamic Light Scattering (DLS)

Samples were analysed using a Malvern Zetasizer Nano ZS instrument with a 4 mW He-Ne solid-state laser operating at 633nm and RI detector at 173°. The instrument was equipped with an integrated Peltier temperature control device with accuracy of ±0.1°C. The formation of L<sub>0.5</sub>-pNIPAM<sub>4.5</sub> particles was monitored by replicating the procedure described in 2.2.1 and 2.2.2 in a quartz cuvette placed into the pre-heated instrument set at 80°C. The intensity-average diameter was measured every 5 minutes and the polymerisation was allowed to proceed for 6 h. The L<sub>0.5</sub>-pNIPAM<sub>4.5</sub> dispersion was then cooled at a rate of 0.33°C/min to 25°C and measurements were collected every 1°C. In order to avoid dust contamination, the solutions were passed through a syringe filter with pore size of 20 µm immediately prior to heating.

#### 2.3.2 UV-Vis spectrophotometry

Transmission spectra, at a wavelength of 260nm, were collected at 2°C decrements between 50 and 20°C using a Cary UV-Vis spectrophotometer (Agilent, USA) using 18 MΩ water as a blank. The samples were allowed to equilibrate in a thermostatically controlled water bath for 30 minutes at each temperature prior to spectrum collection.

#### 2.3.3 Differential scanning calorimetry (DSC)

Calorimetric analysis was performed using a Perkin Elmer DSC 8000 equipped with Pyris Manager software. The samples were heated in sealed aluminium crucibles between 20 to 50°C and cooled back to 20°C at 2°C/min heating and cooling rates.

#### 2.3.4 Rheology

The rheological properties of L<sub>x</sub>-pNIPAM<sub>y</sub> hydrogels were characterised using an Anton Paar 301 rheometer with parallel plates configuration (PP PP50-SN16861 measuring system, 1 mm gap size) in a humidified chamber. Three types of oscillatory measurements were performed in the following order: temperature sweep, frequency sweep and amplitude (strain) sweep. Prior to any

measurements, samples were allowed to reach equilibrium at 50°C for 2 minutes. The temperature sweep was conducted at 1% strain and 10 Hz between 50 to 25°C (2°C/min). The frequency and strain sweeps were conducted at 25°C between 0.01-100 Hz (with 1% strain) and 0.01-1000% strain (at 10 Hz), respectively.

To evaluate the flow behaviour of the L<sub>x</sub>-pNIPAM<sub>y</sub> hydrogels, rotational shear experiments were carried out at different temperatures. Initially, the temperature of the bottom plate was maintained at 50°C for 2 minutes for the temperature of the hydrogel to equilibrate and then cooled to 40°C at 2°C/min. After another 2 minutes of equilibration at this temperature, a rotational shear test was carried out with the shear rate ranging between 0.01 to 100 s<sup>-1</sup>. The same procedure was repeated at 39 and 38°C.

#### 2.3.5 Dynamic Mechanical Analysis (DMA)

DMA was conducted in triplicate using a PerkinElmer DMA8000 model in compression mode at 25°C, applying a sinusoidal force with a 0.5 mm displacement at frequencies between 1-10 Hz. Liquid hydrogels were freshly prepared and solidified as a 4mm thick sheet at room temperature (2h), and a circular biopsy punch (4.5 mm i.d.) was used to remove cylindrical samples from the solid hydrogel. Sample dimensions were confirmed using digital callipers prior to measurement.

#### 2.3.6 Scanning Electron Microscopy (SEM)

Paired samples prepared for DMA analysis were further characterised using SEM. Samples were flash frozen at -80°C and subsequently freeze dried using a FD-1A-50 Freeze Drier set to -53°C, 3.8 x 10<sup>-4</sup> mbar for 8h. The sample was fractured to expose the interior surface morphology, attached onto an aluminium stub and gold coated (10 µA sputter current for 180 s with a 2.7 tooling factor) for imaging. Fracture surfaces were examined using a FEI NOVA nanoSEM 200 scanning electron microscope (SEM). Secondary electron (SE) images were obtained using an accelerating voltage of 5 kV at magnifications ranging from 1000x to 40,000x. For each sample a minimum of six SEM images were collected and examined.

#### 2.3.7 FTIR imaging

Infrared images were collected using an Agilent 680-IR FT-IR spectrometer coupled with a liquid nitrogen cooled mercury cadmium telluride focal plane array detector MCT-FPA (64x64 pixels) and capable of simultaneously collecting 4096 spectra from an image area of 640 µm x 640 µm using the Golden Gate™ Imaging Single Reflection ATR Accessory (Specac Ltd). Images were collected as the average of 64 scans at 4 cm<sup>-1</sup> resolution. Samples were deposited hot, directly onto the ATR crystal and allowed to dry under ambient conditions for 16h prior to data collection.

### 3. Results and discussion

The strategy based on thermally initiated, precipitation polymerisation performed in the presence of dispersed Laponite® platelets results in the synthesis of an easily processable hydrogel system at elevated temperatures that can be injected through fine bore needles, and upon cooling solidifies irreversibly without the need for additional, potentially toxic, reactive moieties<sup>17</sup>. As a polymerised, low

viscosity liquid that does not require further purification after polymerisation and supports cell viability, the  $L_x$ -pNIPAM $_y$  hydrogel was initially developed as an injectable scaffold to support mobility and differentiation of human mesenchymal stem cells for musculoskeletal applications<sup>41–44,46,47</sup>. Whilst  $L_x$ -pNIPAM $_y$  hydrogel compositions have also been shown capable of supporting intestinal epithelium cells in vitro, supporting intestinal crypt culture and modelling inflammatory bowel disease<sup>48–50</sup>. The range of tunability has been shown to support extracellular matrix deposition commensurate with the tissue of interest<sup>41–43,46–50</sup>. This study was designed to provide a better understanding of the polymerisation, solidification, thermal behaviour and mechanical properties of the  $L_x$ -pNIPAM $_y$  hydrogel and some of the composition variations used to tune its mechanical properties.

### 3.1 Empirical observations

After polymerisation at 80°C and while being kept above LCST,  $L_x$ -pNIPAM $_y$  hydrogel behaved as a free-flowing milky suspension (Figure 1a). Upon cooling below the LCST, this milky suspension transformed to an optically transparent hydrogel (Figure 1b). We attribute this to the pNIPAM chains transformation from the globule to the coil conformation and the extension of these chains from the Laponite<sup>®</sup> surface. We hypothesize that in this unfolded coil conformation, the polymer chains form a large number of water-polymer interactions *via* their amide groups, including interactions taking place via bridging water molecules. These interactions are dynamic and permit the high extensibility and good compressibility previously reported by Haraguchi for similar materials synthesised via a different method<sup>51</sup>. The solidified hydrogel did not return to its liquid form upon reheating; instead, it displayed evidence of hydrophobically-induced chain collapse resulting in macroscopic shrinkage (Figure 1c). The key difference between the materials described in this paper and those described by Haraguchi *et al.*<sup>38,51–53</sup> is that by synthesising the  $L_x$ -pNIPAM $_y$  above the LCST using a thermal initiator, a low viscosity and processable liquid is created prior to solidification.

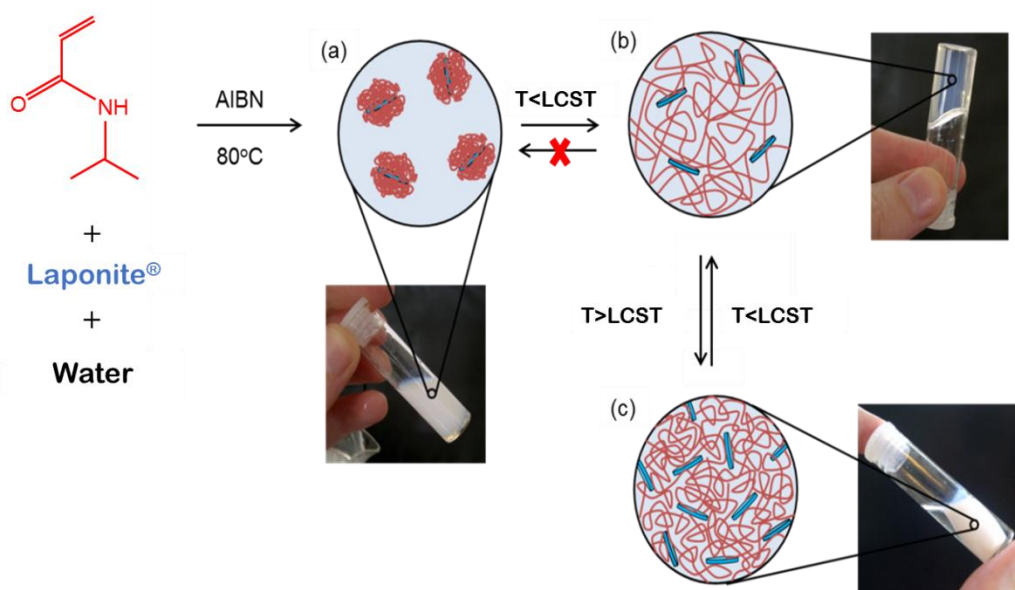


Figure 1. Representative scheme of the a) polymerisation, b) solidification and c) subsequent phase transition behaviour of  $L_x$ -pNIPAM $_y$  nanocomposite materials.

### 3.2 Particle size characterisation

Evidence to support the proposed mechanism for formation of  $L_x$ -pNIPAM $_y$  hydrogels was obtained by monitoring the polymerisation of NIPAM in the presence of Laponite<sup>®</sup> ( $L_{0.5}$ -pNIPAM $_{4.5}$ ) at 80°C, and subsequent cooling, was *in situ* using DLS. The hydrogel composition studied using DLS was selected to replicate the Laponite<sup>®</sup> to NIPAM ratio of our 'standard' hydrogel formulation ( $L_{1.0}$ -pNIPAM $_{9.0}$ ), as the standard formulation was deemed to be too high in concentration to provide reliable DLS measurements. The evolution of the intensity-average diameter with time for dispersions of  $L_{0.5}$ -pNIPAM $_{4.5}$ , NIPAM (pNIPAM $_{5.0}$ ) and Laponite<sup>®</sup> ( $L_{0.5}$ ) held at 80°C in the presence of AIBN initiator are presented in Figures 2a, c and e, respectively, and while cooling to 25°C (Figures 2b, d and f).

NIPAM was polymerised in the presence of Laponite<sup>®</sup> particles (Figure 2a) in a quartz cuvette placed into the pre-heated instrument set at 80°C. The recorded diameter at  $t_0$  (31 nm) is that of the clay particles, as they dominate the scattering of light. After 30 minutes at 80°C the intensity-average diameter increases and the particle size distribution shifts; this coincides with the timescale of pNIPAM $_{5.0}$  polymerisation then precipitation and can be reasonably attributed to the formation of clay-pNIPAM particles. Indeed, the absence of any  $\mu$ m-sized latex particles supports the formation of nanosized hydrogel/Laponite<sup>®</sup> particles. Even at this relatively low aqueous concentration of Laponite<sup>®</sup>, if all the layers were delaminated and dispersed, they would offer a surface area near 800 m<sup>2</sup> g<sup>-1</sup> distributed over 10<sup>20</sup> platelets thus providing an extensive number of potential locations for polymer nucleation and/or adsorption. As time progresses the intensity-average diameter gradually increases to 75nm and the clay-pNIPAM particles can be seen to be colloidally stable, as judged by the monomodal particle size distribution and lack of particle sedimentation in the cuvette. Nelson and Cosgrove<sup>54</sup> reported that adsorption of poly(ethylene oxide) on the surface of Laponite<sup>®</sup> may result in the interparticle interactions becoming much less attractive because of steric repulsion from the adsorbed layers. However, they did not rule out changes in the distribution of the counterions in the electric double layer given that any displacement of these ions would result in a more extended double layer leading to greater electrostatic repulsion. As the pNIPAM chains are insoluble at 80°C, colloidal stability is likely imparted by the hydrophilic clay. Upon cooling (Figure 2b) the intensity-average diameter of the clay-pNIPAM particles remains constant (75 nm) until the LCST of pNIPAM is reached ( $\approx$ 34°C). At this point the globular pNIPAM on the Laponite<sup>®</sup> surfaces transform to the coil conformation, partially extend outward into the aqueous phase and form physical interactions and entanglements with neighbouring clay-pNIPAM particles. The spike in the reported intensity average diameter is indicative of this change.

In the absence of Laponite<sup>®</sup>, NIPAM in the presence of AIBN initiator transforms from a non-scattering suspension at  $t_0$  with a reported diameter  $\approx$ 200nm (Figure 2c), to a highly scattering dispersion of pNIPAM with an intensity-average diameter exceeding 3 $\mu$ m. This dramatic change is caused by the precipitation of water-insoluble pNIPAM chains as micron-sized latex particles. On cooling to 34°C (Figure 2d) the pNIPAM particles transform from the globule to the coil conformation resulting in the

diameter reported by DLS to be large and erroneous and is realistically attributed to the hydration/swelling of the high molecular weight pNIPAM chains.

When aqueous Laponite® is heated and cooled in the absence of NIPAM, the observed intensity-average diameter remains relatively stable with an increase in diameter over time (from 29 to 69 nm). Analysis of the particle size distributions (see inset in Figure 2e) indicates that change in diameter is probably due to an increase in particle aggregation<sup>55</sup>. The initial intensity-average diameter of the pristine Laponite® is approximately 29 nm which is in excellent agreement with the value of 30 nm from neutron scattering<sup>54</sup>. There is no evidence that Laponite® particles became more dispersed upon cooling (Figure 2f).

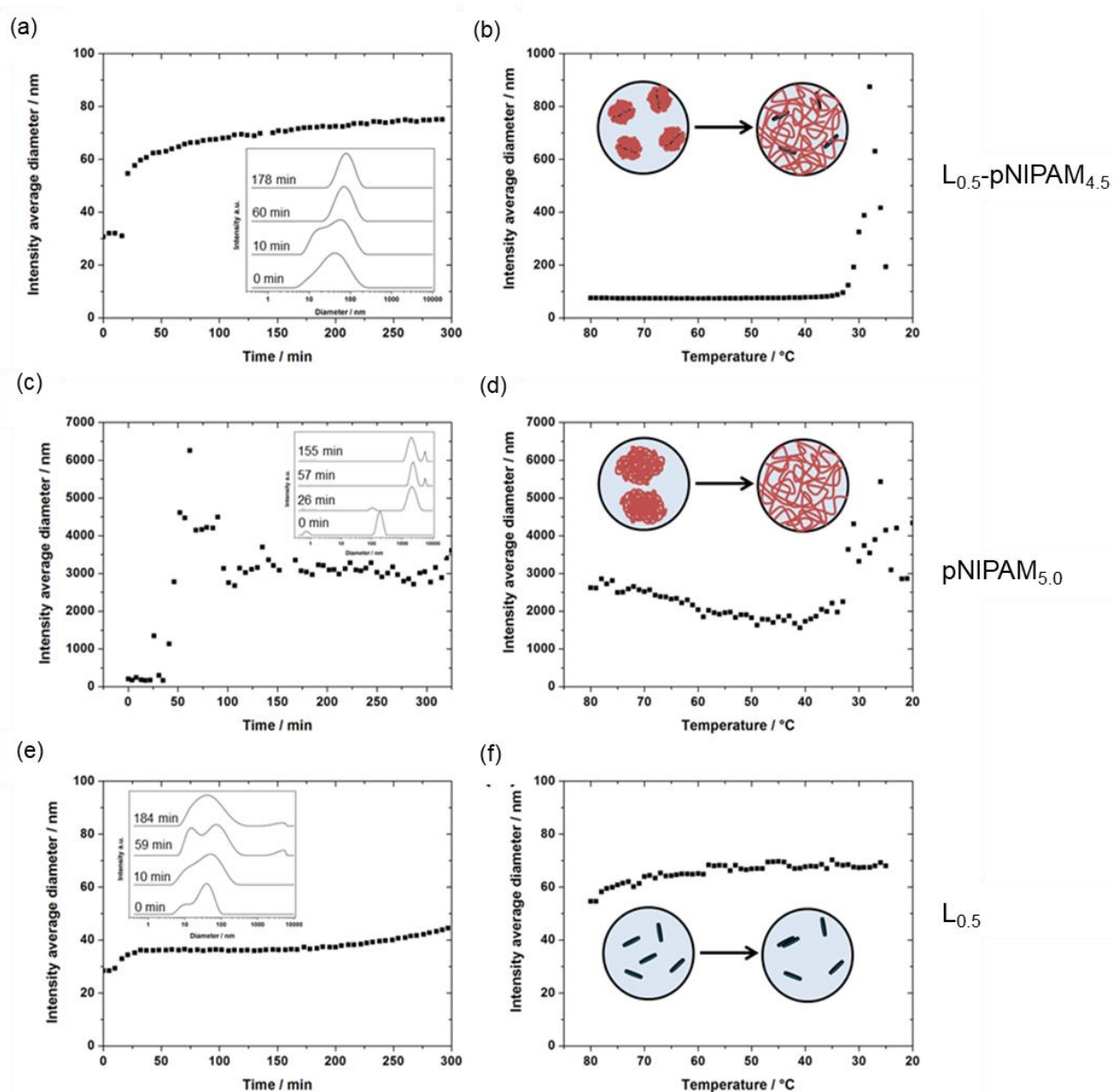


Figure 2. Real time intensity-average diameter of NIPAM/Laponite®/water ( $L_{0.5}$ -pNIPAM<sub>4.5</sub>), NIPAM/water (pNIPAM<sub>5.0</sub>) and Laponite®/water ( $L_{0.5}$ ) maintained at 80°C for 6 hours (a, c and e) and

subsequently cooled at a rate of 0.33°C/min (b, d, and f). The insets show particle size distributions obtained at times indicated and schematics of the proposed structures and transitions.

### 3.3 Controlling the LCST

Several authors<sup>30,56–61</sup> have shown that the LCST of pNIPAM can be effectively controlled through the incorporation of comonomers, and that a linear relationship exists between the LCST and the volume fraction of NIPAM within the copolymer. Principally, a thermoreversible coil-to-globule transition involves interactions between the polymer and solvent which results in the changes in entropy ( $\Delta S_m$ ) and enthalpy ( $\Delta H_m$ ) of mixing becoming more negative. If thermally-induced phase separation is to occur in aqueous solutions, the relative magnitudes of  $\Delta S_m$  and  $\Delta H_m$  must be sufficient to cause a reversal in the sign of the change in Gibbs free energy,  $\Delta G_m$ , at temperatures below 100°C<sup>60–62</sup>. This phase transition is associated with the balance between hydrogen bonding and the hydrophobic interactions between the polymer and water. The LCST of pNIPAM (for coil to globule transition) is well documented in literature<sup>63,64</sup> and is commonly defined as the temperature at which hydrogen bonds break. In this work, the globule-to-coil transition (associated with the formation of hydrogen bonds) of L<sub>x</sub>-pNIPAM<sub>y</sub> hydrogels with and without DMAc are investigated using turbidity, calorimetry and rheology techniques.

As the globule-to-coil transition is accompanied by a dramatic change in turbidity, optical transmission measurements using UV-Vis can provide means for monitoring this transition in real time. The measured LCST (i.e., the temperature at the slope midway point in the transmittance versus T profile) for liquid L<sub>1.0</sub>-pNIPAM<sub>9.0</sub> (or L-pNIPAM-co-DMAc<sub>0</sub>) and L-pNIPAM-co-DMAc<sub>13</sub> as they cooled to room temperature (Figure 3) were 31.2°C and 37.0°C, respectively. The marked increase in transmittance at their respective cloud points with decreasing temperature is attributed to the transformation of the liquid from an optically opaque colloidal suspension containing large, collapsed polymer/clay particles, to a three-dimensional polymer/clay entangled hydrogel network, capable of light transmission. The presence of haze in the L-pNIPAM-co-DMAc<sub>13</sub> gel after solidification, causing a lower % transmittance at T < LCST, was caused by the inhomogeneity in domain/pore size, clearly visible in the SEM images shown in section 3.6 (Figure 8). We theorise that the incorporation of the hydrophilic monomer (DMAc) inhibits complete chain collapse above the LCST and interferes with the free movement of pNIPAM chains during the phase transition, resulting in different aggregation structures. Similar measurements were conducted for samples containing up to 20% DMAc (of the overall polymer content). The LCST of these materials are given in Table 2. The addition of more DMAc into the reaction mixture resulted in the LCST of the copolymer increasing in a dose-responsive manner, in agreement with a trend reported by Barker *et al.*,<sup>30</sup>. The L-pNIPAM-co-DMAc<sub>13</sub> gel has an LCST<sub>peak</sub> (or T<sub>peak</sub>) of ≈37.0°C, which is ideal for injectable therapeutic applications.

However, referring to LCST as a single temperature can be misleading. Variation of the balance between the polymer-polymer interaction and polymer-water interactions can be more accurately described using T<sub>onset</sub> and T<sub>endset</sub> as well as T<sub>peak</sub>. Sensitive measurement techniques are required to detect the T<sub>onset</sub> and T<sub>endset</sub> associated with LCST range.

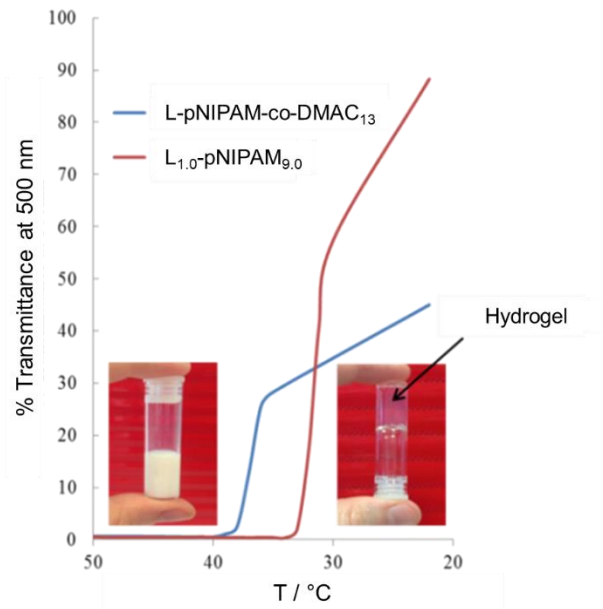


Figure 3. The increase in 260nm light transmittance as the temperature of L<sub>1.0</sub>-pNIPAM<sub>9.0</sub> and L-pNIPAM-co-DMAC<sub>13</sub> liquid hydrogel formulations are reduced (photographs obtained using a L<sub>1.0</sub>-pNIPAM<sub>9.0</sub> formulation; Table 1).

Calorimetry analysis enables monitoring of the formation and breaking of hydrogen bonds within the thermosensitive polymer system as a function of temperature. The exothermic heat flow (between 50-26°C) of the hydrogels containing 0-20% DMAc are displayed in Figure 4. The  $T_{\text{onset}}$ ,  $T_{\text{endset}}$  and  $T_{\text{peak}}$  were evaluated using the exothermic and endothermic peaks (as summarised in Table 2). While the increase in the  $T_{\text{peak}}$  with DMAc content closely resembles the UV-Vis data, it is important to highlight that the LCST range broadens with higher DMAc content. The  $T_{\text{onset}}$  and  $T_{\text{endset}}$  become barely discernible for pNIPAM-co-DMAC<sub>20</sub> indicating that monitoring the LCST range using DSC becomes challenging at higher DMAc content.

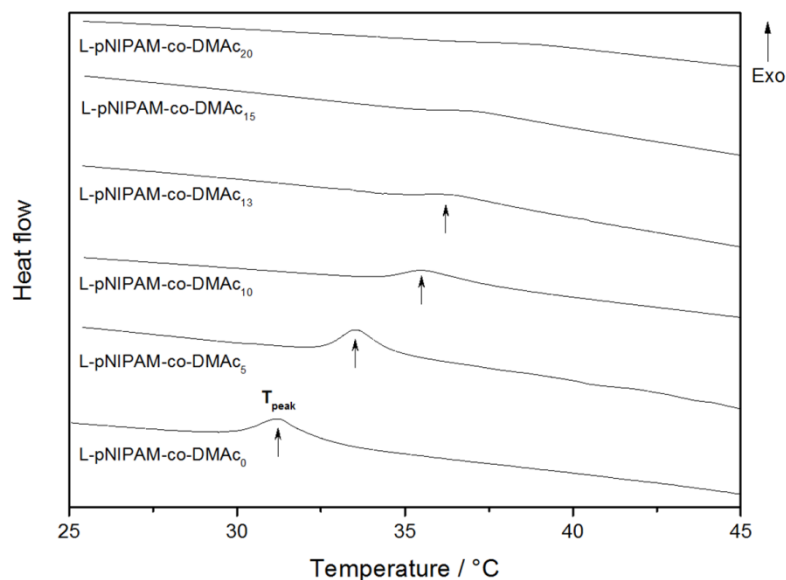


Figure 4. Stacked DSC curves of L<sub>x</sub>-pNIPAM<sub>y</sub> hydrogels with 0-20% DMAc content. The arrows mark the exothermic  $T_{\text{peak}}$ .

Rheology is highly sensitive to the structural changes of a given material (in this case, polymer chain entanglements associated with the phase transition). The storage modulus variations of the different hydrogel systems as a function of temperature are shown in Figure 5a. The addition of DMAc had a noticeable impact on the modulus values of the hydrogels, with L<sub>1.0</sub>-pNIPAM<sub>9.0</sub> displaying the largest storage modulus (>1500 Pa) at 25°C compared to the other systems containing the comonomer. Haraguchi *et al.*<sup>52</sup> reported a similar observation for pDMAc-clay nanocomposites prepared near room temperature compared with their pNIPAM counterparts. The difference in interior morphology and pore structure of the hydrogels could explain this observation. This topic is further explored in section 3.6.

The 1<sup>st</sup> derivative of storage modulus can be used to detect the  $T_{peak}$  more clearly which is defined as the temperature at the point of greatest modulus gradient (Figure 5b). For L<sub>1.0</sub>-pNIPAM<sub>9.0</sub> hydrogel with no DMAc, a sharp rise in modulus is observed at 29.7°C indicating a sudden phase transition at this temperature. Similar to the observation made using DSC, when more DMAc is present in the polymeric chain, the phase transition occurs more gradually. García-Peñas *et al.* reported a similar observation for a pNIPAM-co-dopamine methacrylamide system<sup>31</sup>. Increased hydrophilic interactions caused by the presence of DMAc chains promotes a longer phase transition process and broadens the LCST range. Therefore, presence of hydrophilic DMAc copolymer not only shifts  $T_{peak}$  to higher temperatures but also causes the phase transition process to occur over a longer period. Interestingly, the thermal and rheological behaviour of L<sub>x</sub>NIPAM<sub>y</sub> hydrogel remains consistent even in polymerised suspensions held at 60°C several weeks after polymerisation (Figure S1 of the supplementary data).

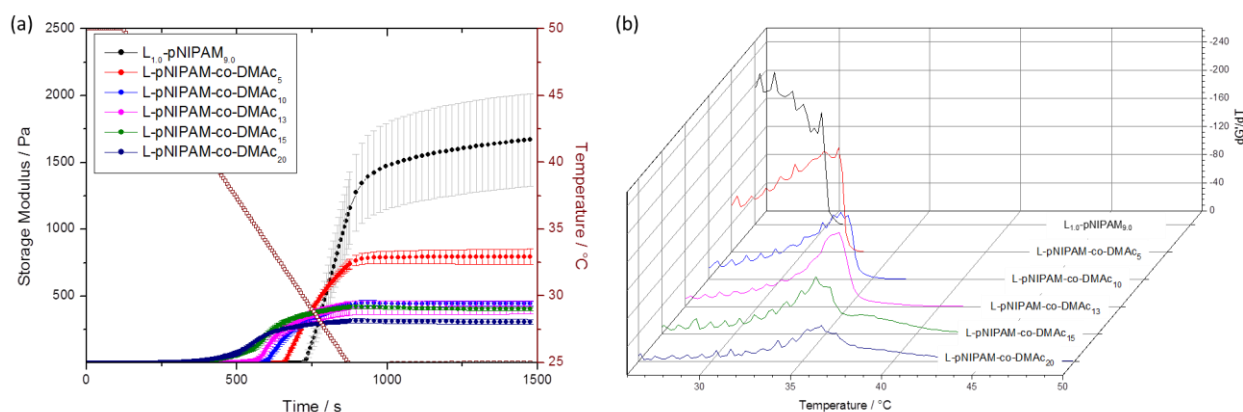


Figure 5. Variation of (a) (average) storage modulus and (b) its 1<sup>st</sup> derivative as a function of temperature for L<sub>x</sub>-pNIPAM<sub>y</sub> hydrogels containing 0-20% DMAc (of the overall polymer content).

Table 2. LCST values as determined by UV-Vis transmittance, calorimetry and rheology measurements as a function of DMAc content.

Method	LCST of L <sub>x</sub> -pNIPAM <sub>y</sub> hydrogels [°C]					
	%DMAc content					
	0%	5%	10%	13%	15%	20%
UV-Vis T <sub>peak</sub>	31.2	-	35.0	37.0	39.5	42.0
DSC T <sub>onset</sub> (Exo)	33.1	34.7	37.2	38.0	39.2	40.5
DSC T <sub>peak</sub> (Exo)	31.2	33.5	35.5	36.3	37.1	38.6
DSC T <sub>endset</sub> (Exo)	30.1	32.5	34.3	34.8	35.4	36.0
DSC T <sub>onset</sub> (Endo)	31.8	33.7	35.4	35.7	35.9	36.9
DSC T <sub>endset</sub> (Endo)	33.8	35.8	38.2	38.9	39.5	40.8
Rheology T <sub>peak</sub>	29.7	31.8	33.7	34.4	34.5	36.1

### 3.4 Injectability

To probe the injectability of L<sub>x</sub>-pNIPAM<sub>y</sub> hydrogels, a critical parameter for many tissue engineering applications, their flow behaviour as a function of temperature was examined. The viscosity of L<sub>x</sub>-pNIPAM<sub>y</sub> hydrogels with 0% and 13% DMAc content at 10 s<sup>-1</sup> shear rate was determined (Table 3). The viscosity measurements were conducted at 40, 39 and 38°C, together with vegetable oil for comparison. An increase in the DMAc content caused an increase in the viscosity of the liquid hydrogel. L-pNIPAM-co-DMAc<sub>13</sub> showed a sharp increase in viscosity (>600%) when the hydrogel was cooled from 40 to 38°C, while a ≈76% increase in viscosity was observed for L<sub>1.0</sub>-pNIPAM<sub>9.0</sub> in identical conditions. This observation can be attributed to the increase in T<sub>peak</sub> and the broadening of the LCST range (Table 2) with an increase in the DMAc content.

Table 3. Viscosity of vegetable oil and L<sub>x</sub>-pNIPAM<sub>y</sub> hydrogels with 0% and 13% DMAc at 10s<sup>-1</sup> shear rate.

Sample	Viscosity at 10s <sup>-1</sup> shear rate [mPa.s]		
	40°C	39°C	38°C
Vegetable oil	185	193	202
L <sub>1.0</sub> -pNIPAM <sub>9.0</sub>	13.6 ± 2.8	31.0 ± 4.3	23.9 ± 3.5
L-pNIPAM-co-DMAc <sub>13</sub>	18.4 ± 6.7	29.8 ± 7.4	132.9 ± 53.9

The flow behaviour of L-pNIPAM-co-DMAc<sub>13</sub> hydrogel in the 0.01-100 s<sup>-1</sup> shear rate range is shown in Figure 6a. The hydrogel demonstrates shear-thinning behaviour at the measurement temperatures which is characterised by a drop in viscosity when the shear rate is increased. The flow behaviour of a viscoelastic material can be modelled mathematically using Herschel-Bulkley (HB) model:

$$\sigma = \sigma_0 + K\dot{\gamma}^n$$

where  $\sigma$  is the shear stress,  $\gamma$  is the shear rate,  $\sigma_0$  is the yield stress,  $K$  is the consistency index and  $n$  is the flow behaviour index. For shear-thinning materials, the  $n$  value must be less than 1<sup>65</sup>. The flow curve for L-pNIPAM-co-DMAc<sub>13</sub> hydrogel at 40°C can be fitted using the HB model (as shown in Figure 6b) with an  $n$  value of 0.53, confirming the shear-thinning behaviour of this material.

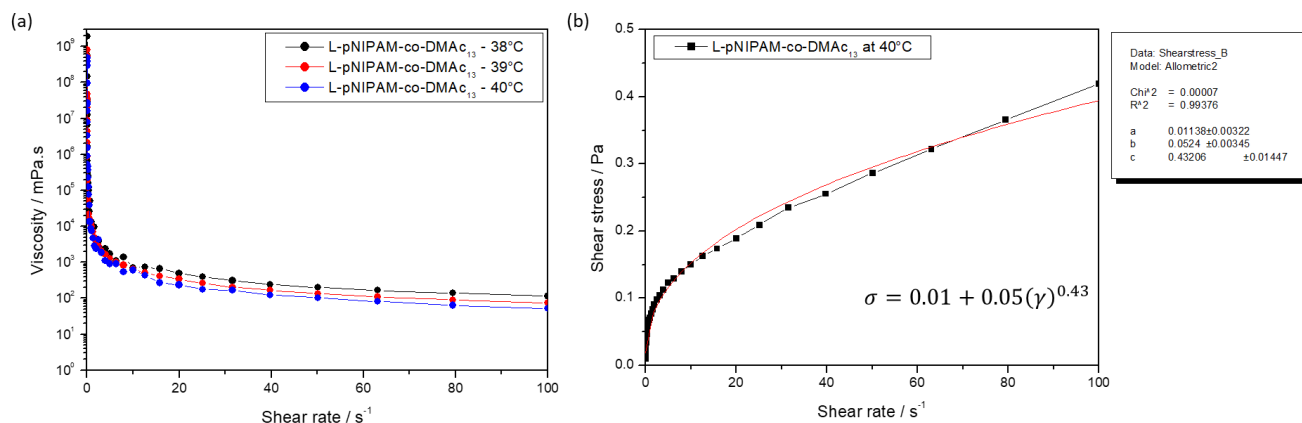


Figure 6. (a) The flow curve and of L-pNIPAM-co-DMAc<sub>13</sub> samples at 40, 39 and 38°C. (b) L-pNIPAM-co-DMAc<sub>13</sub> shear stress vs. shear rate at 40°C fitted using the HB model. The fitting was done using Origin software.

### 3.5 Rheological properties of L<sub>x</sub>-pNIPAM<sub>y</sub> as a function of DMAc content

The influence of DMAc content on the rheological behaviour of the L<sub>x</sub>-pNIPAM<sub>y</sub> hydrogels were investigated using frequency and strain sweep experiments. Frequency sweeps were used to investigate the time-dependent behaviour of the samples in the non-destructive deformation range (within the linear viscoelastic region or LVE). High frequency simulates fast motion on short timescale and low frequency mimics slow motion on long timescales or at rest. The loss modulus ( $G''$ ) and storage modulus ( $G'$ ) values between 0.01-100 Hz (at 1% strain) are displayed in Figure 7a and b. The loss modulus for all hydrogels shows greater frequency dependency compared to their storage modulus which indicates that the viscous behaviour dominates the hydrogel response to frequency variations rather its elastic behaviour. At 25°C and within the physiological frequency range (0.1-6 Hz) all hydrogels behave like a viscoelastic solid ( $G' > G''$ ). At 25°C and 0.01 Hz the L<sub>1.0</sub>-pNIPAM<sub>9.0</sub> hydrogel (containing 0% DMAc) has a storage modulus of 1340 Pa which is >5 times higher than that of L-pNIPAM-co-DMAc<sub>20</sub>. In addition, deviation of  $G'$  from the plateau frequency response of L<sub>1.0</sub>-pNIPAM<sub>9.0</sub> hydrogel (between 0.01-11 Hz) suggests that the frequency dependency of these hydrogels rises with DMAc content. These indicate that an increase in DMAc content lowers the stiffness of the L<sub>x</sub>-pNIPAM<sub>y</sub> hydrogel and results in a weaker gel.

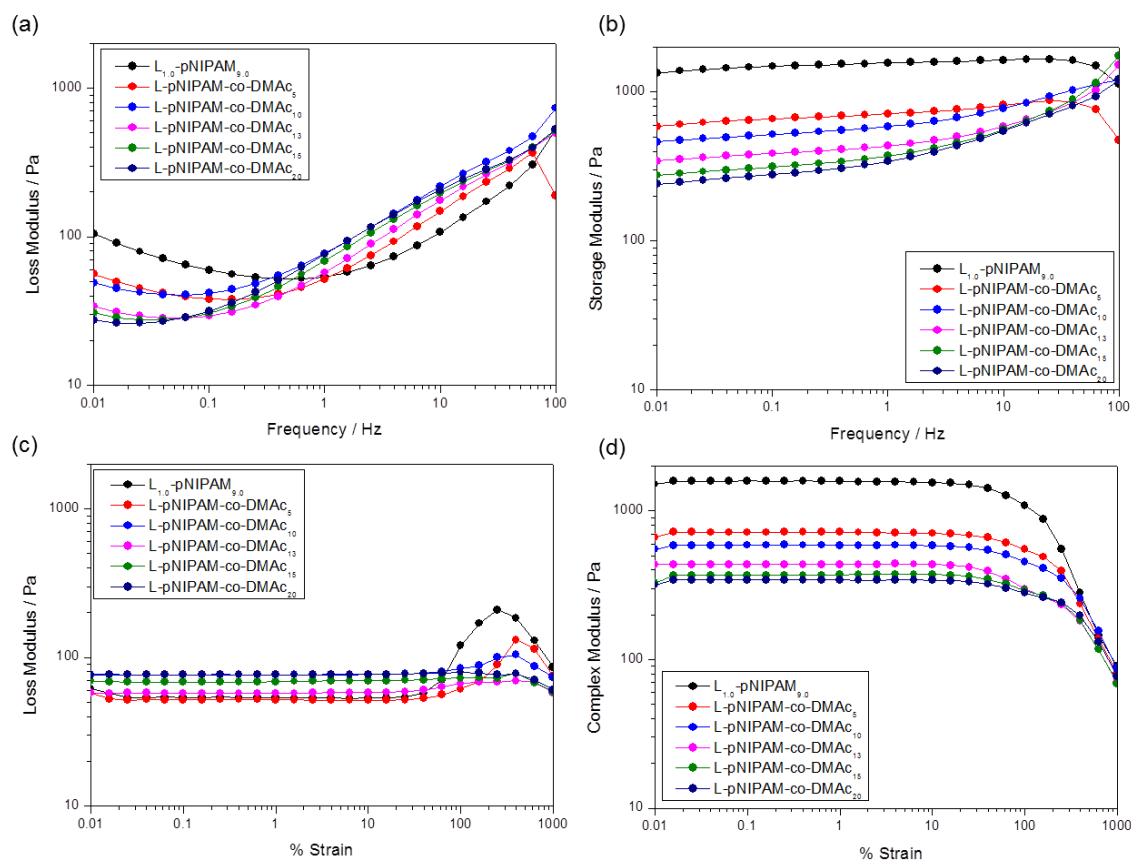


Figure 7. (a) Loss modulus and (b) storage modulus of  $L_x$ -pNIPAM $_y$  hydrogels with different DMAc content in a frequency sweep between 0.01-100 Hz. (c) & (d) show the loss and storage moduli of the same group of hydrogels in a strain sweep experiment with the %strain ranging between 0.01-1000%. All experiments were conducted at 25°C.

Strain sweep data are shown in Figure 7c and d. The LVE region of  $L_x$ -pNIPAM $_y$  hydrogels at 25°C (0.02-11% strain) are not affected by the DMAc content (Figure 7d). The LVE region of the hydrogels are well within the physiological limit. Within this region, all samples can be described as viscoelastic solids since  $G' > G''$ . Similar to the frequency sweep data, hydrogels with lower DMAc content show higher stiffness ( $G'$ ) and therefore, higher structural strength.

### 3.6 Interior morphology

The interior morphology of two solidified hydrogels,  $L_{1.0}$ -pNIPAM $_{9.0}$  and  $L$ -pNIPAM-co-DMAc $_{13}$ , were examined using SEM (Figure 8). The micrographs show that the  $L_{1.0}$ -pNIPAM $_{9.0}$  hydrogel has a comparatively uniform open pore structure with diameters  $\approx 10\mu\text{m}$ . However, the  $L$ -pNIPAM-co-DMAc $_{13}$  hydrogel exhibits smaller pores of two distinct sizes. The first, with a distribution of micropores of diameter  $\approx 5\mu\text{m}$  and the second with a distribution of interconnected nanopores, with diameters  $\approx 100$ -1000nm, at the interfaces between the larger pores. These pores are likely the negative template of ice crystals formed during the freezing process, but still provide a useful marker for the distribution of water within the gels. Cooling rate is known to influence ice crystal size and frequency; however, it is possible that the polymer-water interaction throughout the material is playing a crucial role in governing ice crystal formation. It is likely that the increased hydrophilicity of the co-

polymer material results in a more homogeneous distribution of water and thus, leads to smaller ice crystal formation. The SEM images also suggest that the polymer-clay component forms an extremely fine texture of interconnected thin threads similar to those surrounding 5 $\mu$ m pores in poly(ethyleneoxide)/Laponite<sup>®</sup> hydrogels as described by Loizou *et al.*<sup>66</sup>.

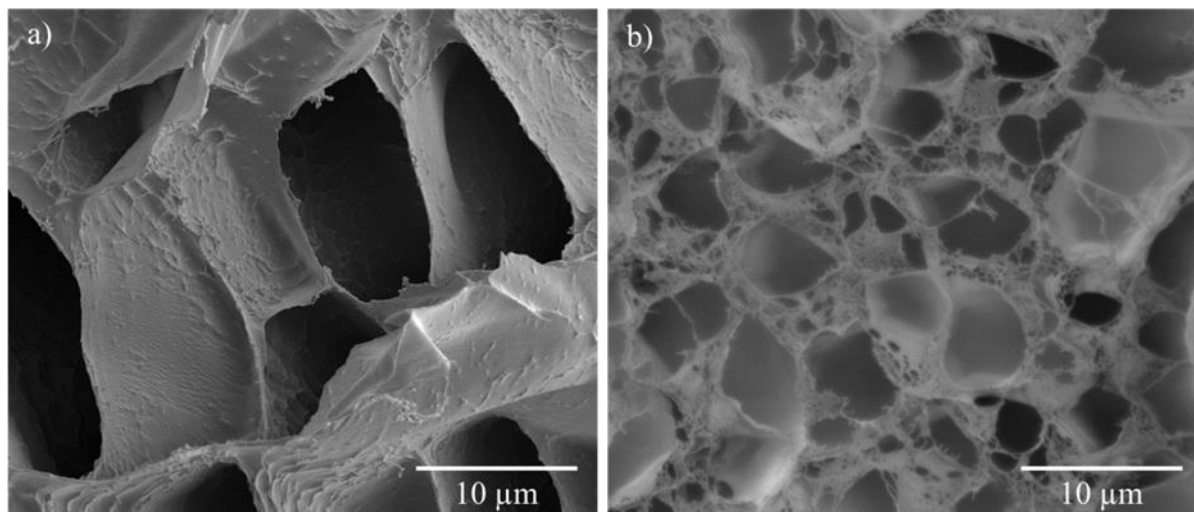


Figure 8. Scanning electron micrographs illustrating the typical interior morphology of a) L-pNIPAM and b) L-pNIPAM-co-DMAc<sub>13</sub> hydrogel.

### 3.7 Processability and inclusion of biologically relevant additives.

To demonstrate ease of processing, 2ml of freshly prepared L<sub>1.0</sub>-pNIPAM<sub>9.0</sub> liquid hydrogel was drawn from its heated reaction vessel (80°C) with a dropping pipette and transferred dropwise to a corrugated heart-shaped steel mould (Figure 9a). Upon cooling to room temperature, the liquid hydrogel quickly (<30 s) solidified; accompanied by a spontaneous change in opacity. When cool, the L<sub>1.0</sub>-pNIPAM<sub>9.0</sub> hydrogel, having taken the precise shape of the complex mould, was easily removed (Figure 9b).

The ease with which biologically relevant additives (in this instance gelatin and PLGA as examples) could be incorporated into the liquid hydrogel prior to solidification is demonstrated in Figure 9c-f. It is worth noting that gelatin is biocompatible, relatively inexpensive, is able to withstand the relatively high temperatures necessary to allow the hydrogel to remain in a liquid state while PLGA is a biodegradable polymer used in a wide range of medical and pharmaceutical applications making both suitable candidates as additives. The trivial dispersion of PLGA microparticles and the homogenous distribution of water soluble gelatin within L<sub>x</sub>-pNIPAM<sub>y</sub> were verified using FTIR imaging in ATR mode. Images were constructed based on the peak height of the  $\delta$ (CH<sub>3</sub>) vibration of pNIPAM (1460 cm<sup>-1</sup>), the  $\nu$ (C=O) vibration of PLGA (1750 cm<sup>-1</sup>) and the amide-III vibration of gelatin (1240 cm<sup>-1</sup>). The  $\delta$ (CH<sub>3</sub>) vibration of pNIPAM was chosen instead of the more commonly used amide I or amide II bands to avoid overlap with gelatin peaks. The distribution of individual PLGA microparticles within PLGA-incorporated hydrogels was discernible (Figure 9d). There was a strong anticorrelation between the pNIPAM domains and the PLGA microparticles with two microparticles recognisable within the measured area. Facile incorporation of active additives (e.g. drug loaded microparticles or

live cells) opens a wide range of possibilities for localised delivery across a range of therapies. In this example, the FTIR-ATR imaging, data show no identifiable gelatin nor pNIPAM rich domains within the gelatin-incorporated specimen (Figure 9e and f), demonstrating that the material is homogenous.

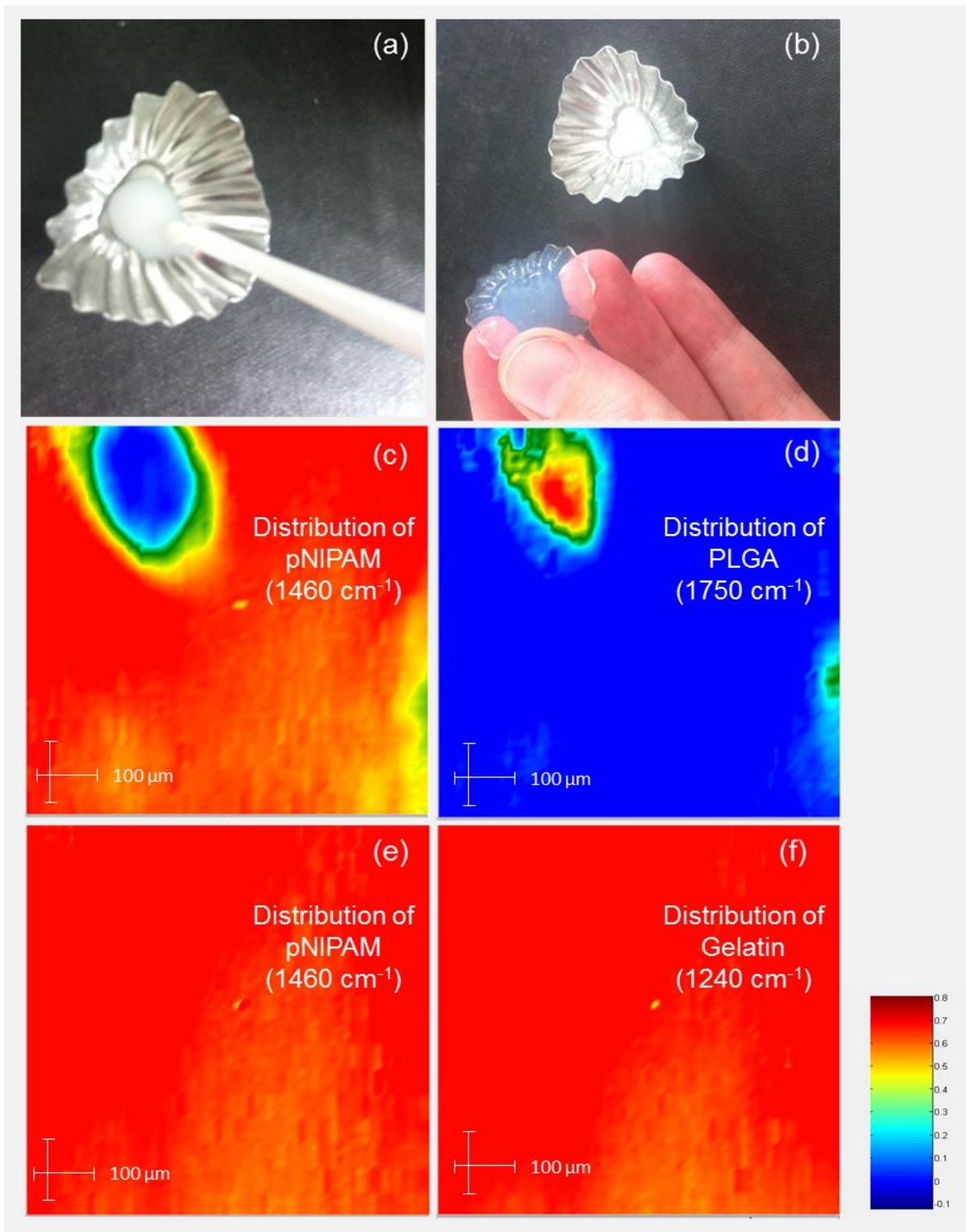


Figure 9. Images showing a)  $L_{1.0}$ -pNIPAM $_{9.0}$  hydrogel immediately prior to solidification and b) the cooled  $L_{1.0}$ -pNIPAM $_{9.0}$  hydrogel. ATR-FTIR images of a dry film of  $L_{0.9}$ -pNIPAM $_{8.1}$ PLGA $_{10}$  highlighting c) pNIPAM distribution ( $\delta(\text{CH}_3)$  vibration), and d) PLGA microparticle distribution ( $\nu(\text{C}=\text{O})$  vibration).

ATR-FTIR images of dry films of  $L_{0.8}$ -pNIPAM $_{7.2}$ G $_{10.0}$  highlighting e) the pNIPAM distribution ( $\delta(\text{CH}_3)$  vibration), and f) the gelatin distribution (amide-III vibration). The colours red and blue indicate areas of the highest and the lowest band intensities, respectively.

### 3.8 Mechanical properties

Dynamic Mechanical Analysis was used in compression mode to investigate the effect of additives (in this instance HA and gelatin as examples) on the mechanical properties of the  $L_x$ -pNIPAM $_y$  hydrogels. Similar to gelatin, the range of important biological functions of HA as well as its structural properties owed to its viscosity and water retention capabilities makes this material another ideal candidate as a hydrogel additive. To account for the additional water incorporated when additives were added, samples prepared by adding the same volume of water,  $L_{0.88}$ -pNIPAM $_{8.0}^{*CTR}$  and  $L_{0.81}$ -pNIPAM $_{7.23}^{*CTR}$  (Table 1), were used as controls. The  $G'$  values for all hydrogel formulations increased with increasing frequency thereby exhibiting typical viscoelastic behaviour (Figure 10a and c).

The addition of HA to  $L_x$ -pNIPAM $_y$  (Figure 10a) caused an overall decrease in  $G'$  values, whereas the control ( $L_{0.81}$ -pNIPAM $_{7.23}^{*CTR}$ ) exhibited a greater degree of linear viscoelasticity during compression, displaying a mechanical behaviour which resembles  $L_{0.9}$ -pNIPAM $_{8.1}$ HA $_{0.2}$  and  $L_{0.8}$ -pNIPAM $_{7.2}$ HA $_{0.4}$  at low frequencies and  $L$ -pNIPAM at higher frequencies. The overall decrease in  $G'$  upon addition of HA to  $L_{1.0}$ -pNIPAM $_{9.0}$  suggests that HA molecules within the hydrogel network interfere with the shear thickening mechanism of the gels at high frequencies. The addition of gelatin to  $L_x$ -pNIPAM $_y$  ( $L_{0.9}$ -pNIPAM $_{8.1}$ G $_{5.0}$  and  $L_{0.8}$ -pNIPAM $_{7.2}$ G $_{10.0}$  in Figure 10c) appeared to reduce  $G'$  although the large error bars temper any firm conclusion. The lowest  $G'$  values were obtained for the Gelatin $_{10}$  sample, suggesting that the change in viscoelastic behaviour of gels containing high concentrations of gelatin are directly linked to the mechanical properties of gelatin and may be the result of gelatin molecules competing with pNIPAM for the clay surface effectively reducing the crosslink density.

The damping ratio ( $\tan \delta$ ) provides information concerning the energy dissipation properties of the gels (in this case as a function of frequency) and is given by the loss modulus/storage modulus ratio, the inelastic and elastic components, respectively. The larger the value of  $\tan \delta$ , the greater the damping force within the material resulting in a reduction of the oscillatory force, which manifests macroscopically as a reduction in the shock of impact. All the formulations exhibit an increase in  $\tan \delta$  at higher frequencies, except for gelatin containing hydrogels, which exhibited similar damping properties to Gelatin $_{10}$  ( $\tan \delta$  does not change with increasing frequency), which implies that the interstitial gelatin is responsible for this property (Figure 10c and d). The addition of HA did not seem to affect the damping properties of these hydrogels. The ability to tune the mechanical properties of the hydrogels could enable lineage selection for differentiation of MSCs towards selected cellular phenotypes which can be regulated by substrate stiffness<sup>67</sup>.

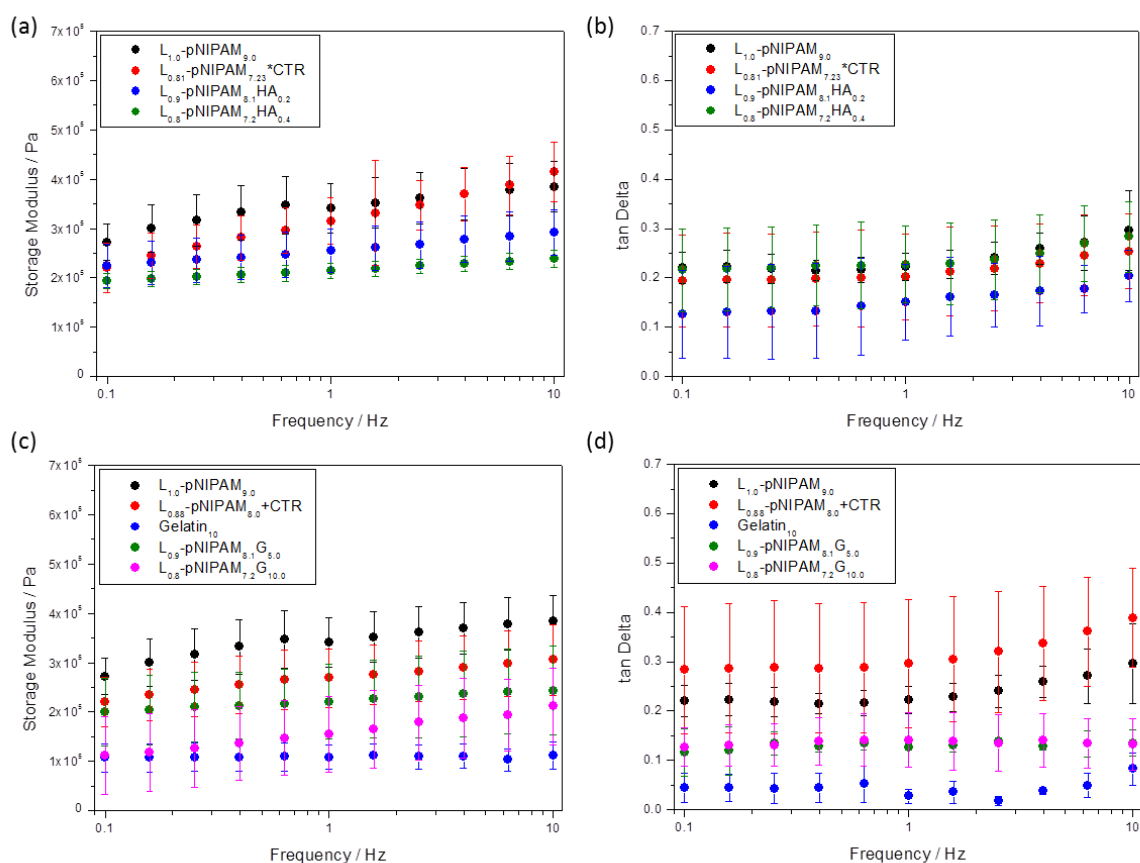


Figure 10. (a & c) Frequency dependency of storage modulus and (b & d) frequency dependence of  $\tan \delta$  for selected  $L_x$ -pNIPAM $_y$  hydrogel formulations and the Gelatin<sub>10</sub> solution.

## 4. Implications for use within regenerative therapies

By exploiting the thermal phase transition of pNIPAM, the  $L_x$ -pNIPAM $_y$  hydrogel can be utilised in innovative ways. The polymer chains remain as discrete colloidal particles immediately following polymerisation and remain so until the material is cooled to a temperature predetermined by the formulation (nature of the copolymer, crosslink density, etc.). This transition is irreversible and the hydrogel does not reliquify upon heating or resuspend upon rehydration (Figure S2). The additional phase in the  $L_x$ -pNIPAM $_y$  production provides opportunities for processing, addition of additives, cell-seeding and injection.

Conventional crosslinked pNIPAM hydrogels demonstrate biocompatibility, but solidify during synthesis and require purification prior to cell plating<sup>38</sup>, both precluding them from injectable delivery systems. The present system allows the suspension of live human cells within the liquid hydrogel<sup>41-43,46,47</sup>. The resulting therapeutic suspension may be administered by injection and completely fill any complex void prior to its solidification<sup>42,43</sup>. This concept is very attractive for therapeutic use in musculoskeletal tissue repair; particularly in clinical cases such as osteoporosis<sup>68</sup> and intervertebral disc degeneration<sup>41,69</sup>, where the use of small bore needles for delivery is necessary to minimise the risk of additional tissue damage<sup>70,71</sup>.

Fundamental design requirements of biomaterial scaffolds are 1) cytocompatibility and 2) the ability to create a cellular environment conducive to synthesis and deposition of extracellular matrix which replicates the composition and structure of the target tissue, consequently inducing the required mechanical properties<sup>72</sup>. Excellent cytocompatibility and induced differentiation of hMSCs to a nucleus pulposus lineage in L-pNIPAM-co-DMAc<sub>13</sub> has been demonstrated<sup>41,42</sup>. In similar studies, differentiation of hMSCs toward osteoblast lineage was demonstrated in L-pNIPAM-co-DMAc<sub>13</sub> containing hydroxyapatite nanoparticles<sup>43,46</sup>. Furthermore, we have shown previously that hMSCs embedded in L-pNIPAM-co-DMAc<sub>13</sub> are induced to synthesize matrix appropriate for musculoskeletal tissues such as the nucleus pulposus of the intervertebral disc<sup>41,42</sup>, or bone<sup>43,46</sup> such as collagens, and proteoglycans which are found in high abundance in these tissues<sup>73-75</sup>. Lineage commitment of MSCs can be mediated by a number of biological, chemical and mechanical cues which can be tailored within biomaterial scaffolds to induce specified types of cellular differentiation. The tuneable mechanical and physiochemical properties possible using this synthetic method via the addition of suitable comonomer and/or additives demonstrates its suitability as a platform scaffold for use in hMSC- targeted regeneration of musculoskeletal tissues.

In addition, microvascular endothelial cells (HDMEC)<sup>46</sup>, colon cancer cell lines (CaCo<sub>2</sub> and HT-29 MTX)<sup>48</sup>, and intestinal crypt stem cells<sup>49</sup> have also been shown to display excellent cytocompatibility within L<sub>1.0</sub>-pNIPAM<sub>9.0</sub> and L-pNIPAM-co-DMAc<sub>13</sub> hydrogels. This has been supplemented with *in vivo* evidence of biocompatibility demonstrating no toxic or adverse effects following subcutaneous implantation or injection to bone<sup>43</sup>.

## 5. Conclusions

We have developed an innovative synthetic route that enables a fully synthesised hydrogel to exist as a free-flowing liquid suspension which irreversibly solidifies upon cooling at a specific, pre-engineered temperature. The method exploits the thermal phase-transition of pNIPAM and its ability to interact with Laponite<sup>®</sup> surfaces. The polymerisation is carried out using an initiating agent which undergoes thermal dissociation at temperatures above which NIPAM will polymerise to form pNIPAM in a hydrophobic, globule conformation. This results in chain propagation close to the Laponite<sup>®</sup> surface, the net result of which is the synthesis of tightly packed polymer chains surrounding each Laponite<sup>®</sup> platelet, where each polymer/clay particle remains discrete from its neighbours. This unique colloidal system remains stable provided the pNIPAM chains are maintained at temperatures above their LCST range. A reduction in temperature to < LCST of the polymer, results in the polymer chains uncoiling and extending away from the clay surfaces enabling them to form bridging interactions with neighbouring clay platelets and entanglements with adjacent uncoiling polymer chains. The final product is a crosslinked, 3-dimensional hydrated polymer network which does not re-liquefy nor cannot be resuspended after drying at elevated temperatures. Solidification requires no additives or additional steps. The mechanical properties and solidification temperature of the materials can be tailored by both the addition of additives and the inclusion of a comonomer. It was also shown that the rate of L<sub>x</sub>-pNIPAM<sub>y</sub> phase transition can be tailored with the comonomer content which may enable

controlled release of therapeutic materials for drug delivery applications. The materials demonstrate excellent potential as a platform technology that may be applied across a range of therapeutic applications.

## Acknowledgements

The authors would like to thank Smith and Nephew Extruded Films and EPSRC (EP/H000275/1, EP/I016473/1), Versus Arthritis, MRC (MR/P026796/1) and this project has received funding from the European Union's Horizon 2020 research and innovation programme under grant agreement No 825925 (iPSpine). We would also like to offer kind thanks to Sheffield Hallam University staff member Stuart Creasey, at the Materials and Engineering Research Institute, for help with the use of the scanning electron microscope.

The authors would like to dedicate this publication to Prof Chris Breen who passed away 13 February 2018.

## Author Contributions

CS, CLM, CB (who passed away Feb 2018), VB, SP, RJ and JF designed experiments. VB conducted the majority of synthesis and characterization experiments, LAF assisted with DLS data collection and led the intellectual discussion of the generated dataset. SP and RJ conducted part of the DMAc range synthesis and the DSC and rheology characterizations. VB, CS, CLM, and RJ co-wrote the manuscript; all authors (except CB) read and approved the final manuscript.

## References

1. Nguyen, Q. V., Huynh, D. P., Park, J. H. & Lee, D. S. Injectable polymeric hydrogels for the delivery of therapeutic agents: A review. *Eur. Polym. J.* **72**, 602–619 (2015).
2. Liu, M. *et al.* Injectable hydrogels for cartilage and bone tissue engineering. *Bone Res.* **5**, 17014 (2017).
3. Sivashanmugam, A., Arun Kumar, R., Vishnu Priya, M., Nair, S. V & Jayakumar, R. An overview of injectable polymeric hydrogels for tissue engineering. *Eur. Polym. J.* **72**, 543–565 (2015).
4. Hou, Q., De Bank, P. A. & Shakesheff, K. M. Injectable scaffolds for tissue regeneration. *J. Mater. Chem.* **14**, 1915–1923 (2004).
5. Temenoff, J. S. & Mikos, A. G. Injectable biodegradable materials for orthopedic tissue engineering. *Biomaterials* **21**, 2405–2412 (2000).
6. Chung, H. J. & Park, T. G. Self-assembled and nanostructured hydrogels for drug delivery and tissue engineering. *Nano Today* **4**, 429–437 (2009).

7. Lu, H. D., Charati, M. B., Kim, I. L. & Burdick, J. A. Injectable shear-thinning hydrogels engineered with a self-assembling Dock-and-Lock mechanism. *Biomaterials* **33**, 2145–2153 (2012).
8. Glassman, M. J. & Olsen, B. D. Structure and mechanical response of protein hydrogels reinforced by block copolymer self-assembly. *Soft Matter* **9**, 6814–6823 (2013).
9. Kharkar, P. M., Kiick, K. L. & Kloxin, A. M. Design of thiol- and light-sensitive degradable hydrogels using Michael-type addition reactions. *Polym. Chem.* **6**, 5565–5574 (2015).
10. Jin, R. *et al.* Synthesis and characterization of hyaluronic acid–poly(ethylene glycol) hydrogels via Michael addition: An injectable biomaterial for cartilage repair. *Acta Biomater.* **6**, 1968–1977 (2010).
11. Lee, Y. *et al.* Thermo-sensitive, injectable, and tissue adhesive sol–gel transition hyaluronic acid/pluronic composite hydrogels prepared from bio-inspired catechol-thiol reaction. *Soft Matter* **6**, 977–983 (2010).
12. Kolb, H. C., Finn, M. G. & Sharpless, K. B. Click Chemistry: Diverse Chemical Function from a Few Good Reactions. *Angew. Chemie Int. Ed.* **40**, 2004–2021 (2001).
13. Takahashi, A. *et al.* In Situ Cross-Linkable Hydrogel of Hyaluronan Produced via Copper-Free Click Chemistry. *Biomacromolecules* **14**, 3581–3588 (2013).
14. Dondoni, A. The Emergence of Thiol–Ene Coupling as a Click Process for Materials and Bioorganic Chemistry. *Angew. Chemie Int. Ed.* **47**, 8995–8997 (2008).
15. Asai, D. *et al.* Protein polymer hydrogels by in situ, rapid and reversible self-gelation. *Biomaterials* **33**, 5451–5458 (2012).
16. Tang, S., Glassman, M. J., Li, S., Socrate, S. & Olsen, B. D. Oxidatively Responsive Chain Extension to Entangle Engineered Protein Hydrogels. *Macromolecules* **47**, 791–799 (2014).
17. Ifkovits, J. L. & Burdick, J. A. Review: photopolymerizable and degradable biomaterials for tissue engineering applications. *Tissue Eng.* **13**, 2369–2385 (2007).
18. Van Tomme, S. R., van Steenberg, M. J., De Smedt, S. C., van Nostrum, C. F. & Hennink, W. E. Self-gelling hydrogels based on oppositely charged dextran microspheres. *Biomaterials* **26**, 2129–2135 (2005).
19. Yan, Y. *et al.* Construction of Injectable Double-Network Hydrogels for Cell Delivery. *Biomacromolecules* **18**, 2128–2138 (2017).
20. Cao, L. *et al.* An injectable hydrogel formed by in situ cross-linking of glycol chitosan and multi-benzaldehyde functionalized PEG analogues for cartilage tissue engineering. *J. Mater. Chem. B* **3**, 1268–1280 (2015).

21. Tan, H., Chu, C. R., Payne, K. A. & Marra, K. G. Injectable in situ forming biodegradable chitosan–hyaluronic acid based hydrogels for cartilage tissue engineering. *Biomaterials* **30**, 2499–2506 (2009).
22. Sakai, S., Hirose, K., Taguchi, K., Ogushi, Y. & Kawakami, K. An injectable, in situ enzymatically gellable, gelatin derivative for drug delivery and tissue engineering. *Biomaterials* **30**, 3371–3377 (2009).
23. Wang, L.-S., Du, C., Chung, J. E. & Kurisawa, M. Enzymatically cross-linked gelatin-phenol hydrogels with a broader stiffness range for osteogenic differentiation of human mesenchymal stem cells. *Acta Biomater.* **8**, 1826–1837 (2012).
24. Dehghan-Niri, M., Tavakol, M., Vasheghani-Farahani, E. & Ganji, F. Drug release from enzyme-mediated in situ-forming hydrogel based on gum tragacanth–tyramine conjugate. *J. Biomater. Appl.* **29**, 1343–1350 (2015).
25. Haines-Butterick, L. *et al.* Controlling hydrogelation kinetics by peptide design for three-dimensional encapsulation and injectable delivery of cells. *Proc. Natl. Acad. Sci. U. S. A.* **104**, 7791–7796 (2007).
26. Bensaïd, W. *et al.* A biodegradable fibrin scaffold for mesenchymal stem cell transplantation. *Biomaterials* **24**, 2497–2502 (2003).
27. Park, K. M. *et al.* Thermosensitive chitosan–Pluronic hydrogel as an injectable cell delivery carrier for cartilage regeneration. *Acta Biomater.* **5**, 1956–1965 (2009).
28. Patenaude, M., Smeets, N. M. B. & Hoare, T. Designing Injectable, Covalently Cross-Linked Hydrogels for Biomedical Applications. *Macromol. Rapid Commun.* **35**, 598–617 (2014).
29. Gao, J. & Frisken, B. J. Influence of Reaction Conditions on the Synthesis of Self-Cross-Linked N-Isopropylacrylamide Microgels. *Langmuir* **19**, 5217–5222 (2003).
30. Barker, I. C. *et al.* Studies of the ‘Smart’ thermoresponsive behavior of copolymers of N-isopropylacrylamide and N,N-dimethylacrylamide in dilute aqueous solution. *Macromolecules* **36**, 7765–7770 (2003).
31. García-Peñas, A. *et al.* Effect of Hydrophobic Interactions on Lower Critical Solution Temperature for Poly(N-isopropylacrylamide-co-dopamine Methacrylamide) Copolymers. *Polymers (Basel)*. **11**, 991 (2019).
32. Jain, K., Vedarajan, R., Watanabe, M., Ishikiriyama, M. & Matsumi, N. Tunable LCST behavior of poly(N-isopropylacrylamide/ionic liquid) copolymers. *Polym. Chem.* **6**, 6819–6825 (2015).
33. Okada, A. & Usuki, A. Twenty Years of Polymer-Clay Nanocomposites. *Macromol. Mater. Eng.* **291**, 1449–1476 (2006).

34. Zhao, L. Z. *et al.* Recent advances in clay mineral-containing nanocomposite hydrogels. *Soft Matter* **11**, 9229–9246 (2015).
35. Lee, W.-F. & Tsao, K.-T. Effect of intercalant content of mica on the various properties for the charged nanocomposite poly(N-isopropyl acrylamide) hydrogels. *J. Appl. Polym. Sci.* **104**, 2277–2287 (2007).
36. Lee, W.-F. & Chen, Y.-C. Effect of bentonite on the physical properties and drug-release behavior of poly(AA-co-PEGMEA)/bentonite nanocomposite hydrogels for mucoadhesive. *J. Appl. Polym. Sci.* **91**, 2934–2941 (2004).
37. Lee, W.-F. & Jou, L.-L. Effect of the intercalation agent content of montmorillonite on the swelling behavior and drug release behavior of nanocomposite hydrogels. *J. Appl. Polym. Sci.* **94**, 74–82 (2004).
38. Haraguchi, K., Takehisa, T. & Ebato, M. Control of Cell Cultivation and Cell Sheet Detachment on the Surface of Polymer/Clay Nanocomposite Hydrogels. *Biomacromolecules* **7**, 3267–3275 (2006).
39. Jain, M. & Matsumura, K. Polyampholyte- and nanosilicate-based soft bionanocomposites with tailorable mechanical and cell adhesion properties. *J. Biomed. Mater. Res. Part A* **104**, 1379–1386 (2016).
40. Chang, C.-W., van Spreeuwel, A., Zhang, C. & Varghese, S. PEG/clay nanocomposite hydrogel: a mechanically robust tissue engineering scaffold. *Soft Matter* **6**, 5157–5164 (2010).
41. Thorpe, A. A., Boyes, V. L., Sammon, C. & Le Maitre, C. L. Thermally triggered injectable hydrogel, which induces mesenchymal stem cell differentiation to nucleus pulposus cells: Potential for regeneration of the intervertebral disc. *Acta Biomater.* **36**, 99–111 (2016).
42. Thorpe, A. A. *et al.* Thermally triggered hydrogel injection into bovine intervertebral disc tissue explants induces differentiation of mesenchymal stem cells and restores mechanical function. *Acta Biomater.* **54**, 212–226 (2017).
43. Thorpe, A. A. *et al.* In vivo safety and efficacy testing of a thermally triggered injectable hydrogel scaffold for bone regeneration and augmentation in a rat model. *Oncotarget* **9**, 18277–18295 (2018).
44. Boyes, V., Sammon, C., Le Maitre, C. & Breen, C. Composite hydrogel-clay particles, Patent i.d: WO2013027051A1. (2013).
45. Jordan, F. *et al.* Sustained release hGH microsphere formulation produced by a novel supercritical fluid technology: In vivo studies. *J. Control. Release* **141**, 153–160 (2010).
46. Thorpe, A. A., Creasey, S., Sammon, C. & Le Maitre, C. L. Hydroxyapatite nanoparticle

- injectable hydrogel scaffold to support osteogenic differentiation of human mesenchymal stem cells. *Eur. Cells Mater.* **32**, 1–23 (2016).
47. Vickers, L., Thorpe, A. A., Snuggs, J., Sammon, C. & Le Maitre, C. L. Mesenchymal stem cell therapies for intervertebral disc degeneration: Consideration of the degenerate niche. *Jor Spine* **2**, 1–14 (2019).
  48. Dosh, R. H., Essa, A., Jordan-Mahy, N., Sammon, C. & Le Maitre, C. L. Use of hydrogel scaffolds to develop an in vitro 3D culture model of human intestinal epithelium. *Acta Biomater.* **62**, 128–143 (2017).
  49. Dosh, R. H., Jordan-Mahy, N., Sammon, C. & Le Maitre, C. L. Use of I-pNIPAM hydrogel as a 3D-scaffold for intestinal crypts and stem cell tissue engineering. *Biomater. Sci.* **7**, 4310–4324 (2019).
  50. Dosh, R. H., Jordan-Mahy, N., Sammon, C. & Le Maitre, C. L. Long-term in vitro 3D hydrogel co-culture model of inflammatory bowel disease. *Sci. Rep.* **9**, 1812 (2019).
  51. Haraguchi, K. & Takehisa, T. Nanocomposite Hydrogels: A Unique Organic–Inorganic Network Structure with Extraordinary Mechanical, Optical, and Swelling/De-swelling Properties. *Adv. Mater.* **14**, 1120–1124 (2002).
  52. Haraguchi, K., Farnworth, R., Ohbayashi, A. & Takehisa, T. Compositional Effects on Mechanical Properties of Nanocomposite Hydrogels Composed of Poly(N,N-dimethylacrylamide) and Clay. *Macromolecules* **36**, 5732–5741 (2003).
  53. Haraguchi, K. & Takehisa, T. Novel manufacturing process of nanocomposite hydrogel for bio-applications. in *ASME 2005 International Mechanical Engineering Congress and Exposition* Haraguchi, K. Takehisa, T. (2005).
  54. Nelson, A. & Cosgrove, T. A Small-Angle Neutron Scattering Study of Adsorbed Poly(ethylene oxide) on Laponite. *Langmuir* **20**, 2298–2304 (2004).
  55. Bergaya, F. & Lagaly, G. *Handbook of Clay Science, Volume 5*. (Elsevier, 2013).
  56. Feil, H., Bae, Y. H., Feijen, J. & Kim, S. W. Effect of comonomer hydrophilicity and ionization on the lower critical solution temperature of N-isopropylacrylamide copolymers. *Macromolecules* **26**, 2496–2500 (1993).
  57. Zhou, Y., Jiang, K., Song, Q. & Liu, S. Thermo-Induced Formation of Unimolecular and Multimolecular Micelles from Novel Double Hydrophilic Multiblock Copolymers of N,N-Dimethylacrylamide and N-Isopropylacrylamide. *Langmuir* **23**, 13076–13084 (2007).
  58. Li, G.-Y. *et al.* Synthesis and self-assembly of temperature- and pH-sensitive diblock copolymer of poly(acrylic acid)-b-poly(N-isopropylacrylamide). **27**, 956–960 (2006).

59. Wintgens, V., Charles, M., Allouache, F. & Amiel, C. Triggering the Thermosensitive Properties of Hydrophobically Modified Poly(N-isopropylacrylamide) by Complexation with Cyclodextrin Polymers. *Macromol. Chem. Phys.* **206**, 1853–1861 (2005).
60. Chee, C.-K. *et al.* Manipulating the thermoresponsive behaviour of poly(N-isopropylacrylamide) 3. On the conformational behaviour of N-isopropylacrylamide graft copolymers. *Soft Matter* **5**, 3701–3712 (2009).
61. Chee, C. K., Rimmer, S., Shaw, D. A., Soutar, I. & Swanson, L. Manipulating the Thermoresponsive Behavior of Poly(N-isopropylacrylamide). 1. On the Conformational Behavior of a Series of N-Isopropylacrylamide–Styrene Statistical Copolymers. *Macromolecules* **34**, 7544–7549 (2001).
62. Shibayama, M., Mizutani, S. & Nomura, S. Thermal Properties of Copolymer Gels Containing N-Isopropylacrylamide. *Macromolecules* **29**, 2019–2024 (1996).
63. Tong, Z., Zeng, F., Zheng, X. & Sato, T. Inverse Molecular Weight Dependence of Cloud Points for Aqueous Poly(N-isopropylacrylamide) Solutions. *Macromolecules* **32**, 4488–4490 (1999).
64. Osa, M. Aqueous Solution Properties of Poly(N-isopropylacrylamide). *KOBUNSHI RONBUNSHU* **66**, (2009).
65. Osswald, T. & Rudolph, N. Polymer Rheology. Fundamentals and Applications. in *Hanser Publications* vol. 37 (Hanser Publishers, 2015).
66. Loizou, E. *et al.* Large Scale Structures in Nanocomposite Hydrogels. *Macromolecules* **38**, 2047–2049 (2005).
67. Burdick, J. A. & Prestwich, G. D. Hyaluronic acid hydrogels for biomedical applications. *Adv. Mater.* **23**, H41-56 (2011).
68. Dimitriou, R., Jones, E., McGonagle, D. & Giannoudis, P. V. Bone regeneration: current concepts and future directions. *BMC Med.* **9**, 66 (2011).
69. Le Maitre, C. L., Binch, A. L., Thorpe, A. A. & Hughes, S. P. Degeneration of the intervertebral disc with new approaches for treating low back pain. *J. Neurosurg. Sci.* **59**, 47–61 (2015).
70. Michalek, A. J., Buckley, M. R., Bonassar, L. J., Cohen, I. & Iatridis, J. C. The effects of needle puncture injury on microscale shear strain in the intervertebral disc annulus fibrosus. *Spine J.* **10**, 1098–1105 (2010).
71. Nassr, A. *et al.* Does incorrect level needle localization during anterior cervical discectomy and fusion lead to accelerated disc degeneration? *Spine (Phila. Pa. 1976)*. **34**, 189–192 (2009).
72. Drury, J. L. & Mooney, D. J. Hydrogels for tissue engineering: scaffold design variables and

- applications. *Biomaterials* **24**, 4337–4351 (2003).
73. Mwale, F., Roughley, P. & Antoniou, J. Distinction between the extracellular matrix of the nucleus pulposus and hyaline cartilage: a requisite for tissue engineering of intervertebral disc. *Eur. Cell. Mater.* **8**, 54–58 (2004).
  74. Roughley, P. Biology of Intervertebral Disc Aging and Degeneration: Involvement of the Extracellular Matrix. *Spine (Phila. Pa. 1976)*. **29**, 2691–2699 (2005).
  75. Weiner, S. & Traub, W. Bone structure: from angstroms to microns. *FASEB J. Off. Publ. Fed. Am. Soc. Exp. Biol.* **6**, 879–885 (1992).

## Supplementary data to the manuscript

### "One-Pot Precipitation Polymerisation Strategy for Tuneable Injectable Laponite®-pNIPAM Hydrogels: Polymerisation, Processability and Beyond."

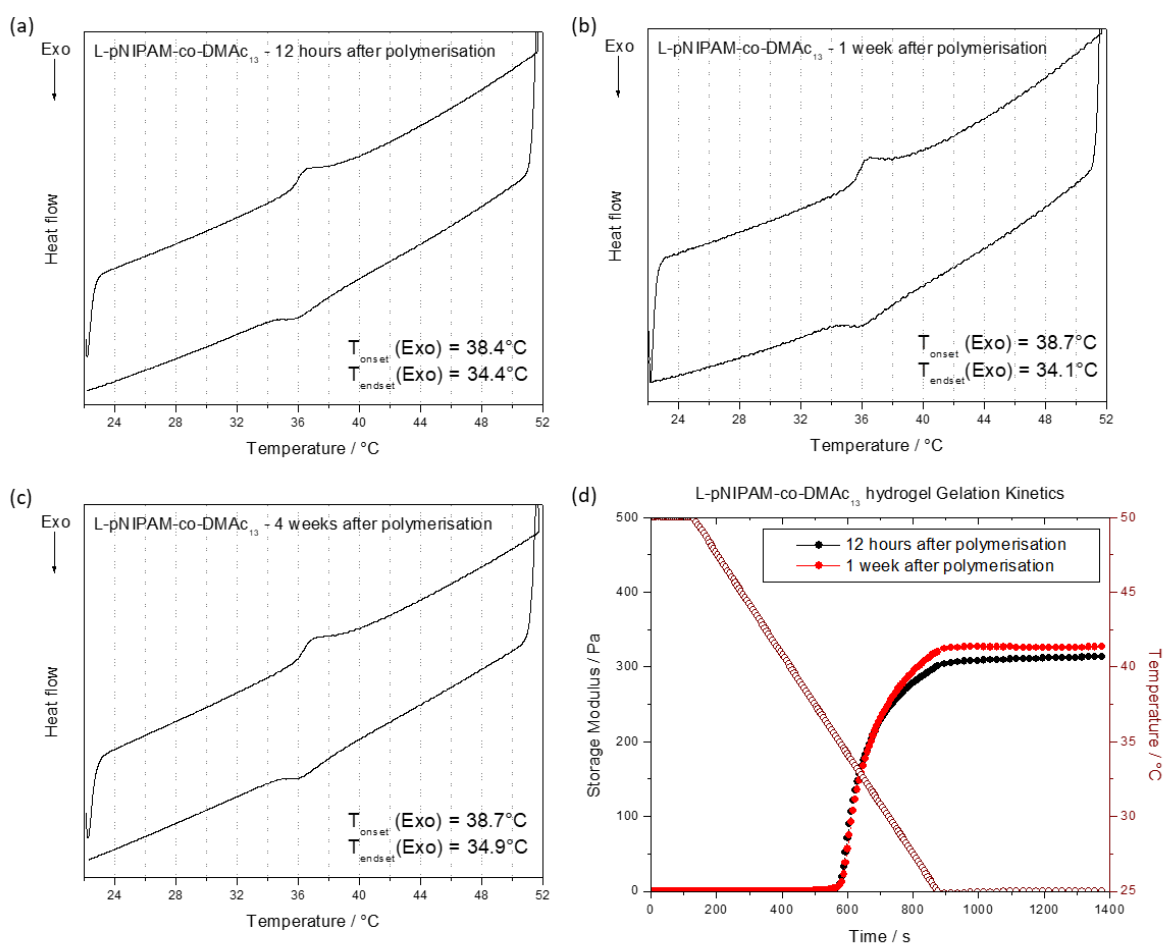


Figure S1 (a-c) The DSC curves of the L-pNIPAM-co-DMAc<sub>13</sub> hydrogel after 12 hours, 1 week and 4 weeks after polymerisation. (d) changes in the storage modulus of L-pNIPAM-co-DMAc<sub>13</sub> hydrogel when cooled from 50°C to 25°C after 12 hours and 1 week of being polymerised.

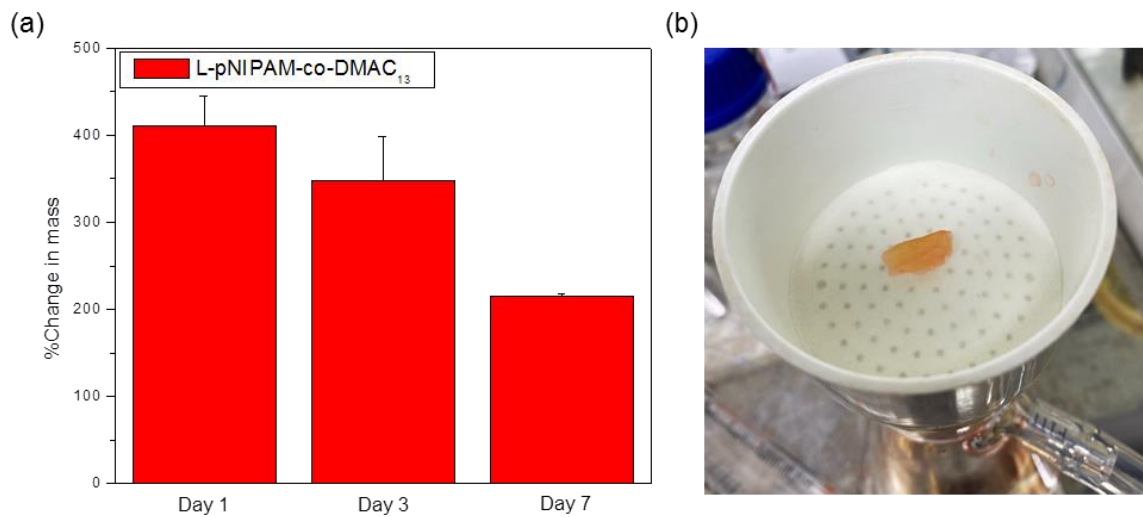


Figure S2 (a) Swelling rate of dried L-pNIPAM-co-DMAC<sub>13</sub> sample in supplemented DMEM medium with 350mOsm/kg osmolarity at 37°C, (b) Image of a hydrogel sample after swelling. The measurements were conducted using the vacuum filtration method.